



Time-varying responses of lake metabolism to light and temperature

Joseph S. Phillips *

Department of Integrative Biology, University of Wisconsin-Madison, Madison, Wisconsin

Abstract

Light is a primary driver of lake ecosystem metabolism, and the dependence of primary production on light is often quantified as a photosynthesis-irradiance or “P-I” curve. The parameters of the P-I curve (e.g., the maximum primary production when light is in excess) can change through time due to a variety of biological factors (e.g., changes in biomass or community composition), which themselves are subject to external drivers (e.g., herbivory or nutrient availability). However, the relative contribution of variation in the P-I curve to overall ecosystem metabolism is largely unknown. I developed a statistical model of ecosystem metabolism with time-varying parameters governing the P-I curve, while also accounting for the influence of temperature. I parameterized the model with dissolved oxygen time series spanning six summers from Lake Mývatn, a shallow eutrophic lake in northern Iceland with large temporal variability in ecosystem metabolism. All of the estimated parameters of the P-I curve varied substantially through time. The sensitivity of primary production to light under light-limiting conditions was particularly variable (>15-fold) and had a compensatory relationship with ambient light levels. However, the 3.5-fold variation in the maximum potential primary production made the largest contribution to variation in ecosystem metabolism, accounting for around 90% of the variance in net ecosystem production. Much of the variation in maximum primary production was attributable to cyanobacterial blooms, which occur in some but not all years in Mývatn. Overall, these results illustrate how changes in the P-I curve contribute substantially to temporal variation in lake ecosystem metabolism.

Ecosystem metabolism, the biological assimilation and release of carbon, is central to the function of aquatic ecosystems (Hanson et al. 2003; Staehr et al. 2010a,b). Photosynthesis stores light energy in the form of organic compounds, and gross carbon assimilation (known as gross primary production or GPP) provides metabolic energy and structural material to primary producers, higher trophic levels, and detrital food webs (Del Giorgio et al. 1999; Carpenter et al. 2001; Chapin et al. 2006). In ecosystems without substantial external carbon inputs, in situ GPP constrains total biological productivity, which in turn influences ecological dynamics across organizational scales (Del Giorgio et al. 1999; Fussmann 2000; Staehr et al. 2010b). The counterpart to GPP is ecosystem respiration (ER), which includes the oxidation of organic carbon and subsequent energy utilization by all organisms in the ecosystem (Chapin et al. 2006; Solomon et al. 2013). The balance between GPP and ER determines the net assimilation or release of carbon due to biological processes (net ecosystem production or NEP), which plays a key role in ecosystem carbon budgets (Randerson et al. 2002; Chapin et al. 2006; Demars et al. 2016).

Freshwater ecosystems can be either sources or sinks of CO₂ and make substantial contributions to regional carbon cycling, especially in landscapes with high densities of freshwater bodies (Cole et al. 2007; Raymond et al. 2013; Demars et al. 2016; Holgerson and Raymond 2016). Therefore, characterizing the physical and biological controls of ecosystem metabolism is important for predicting both the local function and regional impacts of freshwater systems.

Light is a fundamental requirement of photosynthesis, and the dependence of ecosystem metabolism on light is often characterized by photosynthesis-irradiance or “P-I” curves (Jassby and Platt 1976; Behrenfeld and Falkowski 1997; Staehr et al. 2016) (Fig. 1). In this framework, variation in lake metabolism arises from two sources: (1) variation in light levels and (2) variation in the P-I curve. Aquatic ecosystems experience substantial variability in light due to changes in solar irradiance (e.g., diel and seasonal cycles; changes in cloud cover) and water clarity (e.g., resuspension of sediment; phytoplankton blooms). Changes in the P-I curve result from biological processes across organizational scales (Falkowski 1984). At the cellular level, photosynthetic rates vary with temperature, availability of nutrients, and physiological regulation (Falkowski 1984; Davison 1991; Edwards et al. 2011). For example, aquatic primary producers can increase production of photosynthetic pigments with response to chronic light limitation, thereby increasing their sensitivity to a given

*Correspondence: josephsmphillips@gmail.com

Additional Supporting Information may be found in the online version of this article.

amount of light (Falkowski 1984; Moore et al. 2006; Dubinsky and Stambler 2009). At the population and community scale, photosynthetic rates may change due to variation in primary producer biomass, rapid evolution, and species composition (Carpenter and Kitchell 1984; Vrede et al. 2009; Schwaderer et al. 2011; Edwards et al. 2015), which can either occur with response to the physical environment or through interactions with other organisms (e.g., competition with other producers; herbivory by zooplankton) (Carpenter and Kitchell 1984; Bergquist and Carpenter 1986; Yoshiyama et al. 2009; Hashioka et al. 2013).

In addition to variation in photosynthesis (i.e., GPP), changes in respiration (i.e., ER) can also alter P-I relationships. It is common in studies of lake metabolism to assume that ER is independent of variation in light (but see Sadro et al. 2011; Schindler et al. 2017 for discussion of how ER can change with light), which means that variation in ER changes the intercept of the P-I curve (Fig. 1). ER comprises respiration by both autotrophs (i.e., primary producers) and heterotrophs, and so ER is determined in part by their respective biomasses that can vary substantially through time (Del Giorgio et al. 1999). The extent to which heterotrophic production (and therefore respiration) is coupled with GPP is expected to depend on the dominant source of carbon in the system (Del Giorgio et al. 1999; Solomon et al. 2013). Many freshwater ecosystems are dominated by allochthonous (external) sources of carbon, especially those with extensive boundaries along terrestrial landscapes (e.g., streams) (Thorp and Delong 2002; Hoellein et al. 2013). In these ecosystems, heterotrophic respiration (and total ER) can exceed GPP and changes with response to variation in the allochthonous resource (Hanson et al. 2003; Cole et al. 2006; Ask et al. 2009; Staehr et al. 2010b). Conversely, in ecosystems with relatively low allochthonous inputs, ER should be more

strongly coupled to GPP, due to both respiration by primary producers and respiration by heterotrophs whose primary source of carbon is in situ GPP (Solomon et al. 2013). On shorter time scales, ER is driven by variation in temperature (Solomon et al. 2013; Demars et al. 2016; Song et al. 2018), due to the thermal dependence of enzyme kinetics. GPP may also be influenced by changes in temperature, although ER is assumed to be more sensitive to temperature (but see Demars et al. 2016).

Despite the large potential for temporal variation in the P-I curve for NEP due to biological changes in GPP and ER, the relative contribution of this variation to ecosystem metabolism is not fully understood (but see Staehr et al. 2016 for an assessment of variation in light saturation and photoinhibition of metabolism across 15 lakes). In this study, I present a statistical model of ecosystem metabolism with time-varying parameters governing the P-I curve, and I fit the model to observations of dissolved oxygen (DO) from Lake Mývatn in northern Iceland. This approach builds on a large body of work utilizing time series of DO to infer ecosystem metabolism in aquatic systems, relying on the fact that photosynthesis releases oxygen while aerobic respiration consumes oxygen and assuming that respective conversions between CO₂ and O₂ fluxes are approximately equal (Odum 1956; Hanson et al. 2008; Holtgrieve et al. 2010; Staehr et al. 2010a; Richardson et al. 2017). The model includes explicit dependence of GPP and ER on temperature, because temperature is a well-documented driver of the physiological processes contributing to ecosystem metabolism (Demars et al. 2016). Beyond the effects of light and temperature, the parameters of the P-I curve vary smoothly through time as stochastic processes and thereby capture temporal variation in ecosystem metabolism due to changes in the P-I curve itself. These changes could be due to a variety of biological factors (e.g., organismal traits, biomass, or community composition) which themselves could be influenced by changes in other physical and biological variables (e.g., herbivory, nutrient availability, or lake mixing).

I applied this method to DO time series from Lake Mývatn spanning six summers to (1) characterize temporal variation in Mývatn's P-I relationship, (2) evaluate the contribution of this variation to changes in ecosystem metabolism, and (3) evaluate the contribution of different variables to the coupling of GPP and ER. Mývatn is dynamic with much of its ecology being driven by midges (Diptera: Chironomidae) that fluctuate across four orders-of-magnitude and constitute the majority of the lake's secondary biomass production (Einarsson et al. 2004). The midges are ecosystem engineers and locally stimulate both GPP and ER, such that their population fluctuations may contribute to large variation in Mývatn's whole-lake metabolism (Herren et al. 2017; Phillips et al. 2019). Furthermore, while Mývatn is generally dominated by benthic primary production during clear-water phases, it is also subject to cyanobacterial blooms that are occasionally very thick and may shift the majority of production from benthic to pelagic (Einarsson

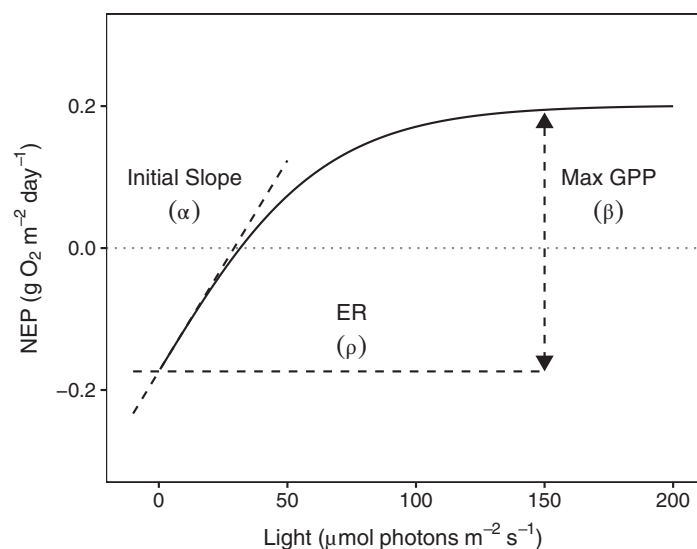


Fig. 1. P-I curve for ecosystem metabolism. The dashed lines illustrate the contribution of each parameter of the P-I curve. The dotted line shows NEP of 0, where GPP equals ER (since $NEP = GPP - ER$).

et al. 2004). The dynamic nature of Mývatn's ecology likely results in large variation in its responses to light and temperature, making it a useful case for partitioning the relative contribution of different sources of variation in ecosystem metabolism.

Methods

Study system

Mývatn is located in the northeast Iceland (65°40 N, 17°00 W), approximately 100 km south of the Arctic Circle and has a tundra-subarctic climate (Björnsson and Jónsson 2004). The lake has two basins (north and south) connected by a narrow channel; the south basin is larger (28.2 km²) and is the central focus of this study. The south basin is shallow (mean depth = 2.3 m; max depth = 4 m) and has a consistent water level and flow rate due to the stability of its groundwater source (Einarsson et al. 2004). Mývatn does not stratify in the summer and its water temperature closely tracks the air temperature (Einarsson et al. 2004). On average, the majority of the south basin is frozen for 190 d per year. Phosphorous- and silicon-rich cold springs (inputs of N, P, and Si = 1.4, 1.5, and 340 g m⁻² yr⁻¹) feed the south basin; water column concentrations are spatially variable but average values for the center of the lake for N, P, and Si are 0.196, 0.0135, and 3.75 mg L⁻¹, respectively (Ólafsson 1979). Consequently, Mývatn is naturally eutrophic with high primary production. According to previous estimates, the majority of primary production is benthic and attributable to benthic diatoms (chiefly Fragilariaceae) and mats of filamentous green algae (*Cladophora glomerata* and *Aegagropila linnai*) (Ólafsson 1979; Einarsson et al. 2004). However, there are occasional blooms of green algae, diatoms, and cyanobacteria which may make substantial contributions to primary production. The cyanobacterial blooms (chiefly *Dolichospermum* spp.) in particular can be quite thick (peak phycocyanin concentration >200 µg L⁻¹), blocking almost all light below 5 cm of the water surface (Phillips et al. 2019). Benthic primary production supports large populations of midges (>30 species) that in peak years compose over two-thirds of the lake's secondary production and show dramatic fluctuations in abundance spanning four orders of magnitude (Lindegård and Jónasson 1979; Einarsson et al. 2004; Ives et al. 2008). The midges in turn are an important food source for ducks and fish (sticklebacks, brown trout, and arctic char). The two dominant midge genera (*Tanytarsus* and *Chironomus*) are tube-building ecosystem engineers that locally stimulate benthic GPP by providing a stable three-dimensional substrate for diatom growth (Hölker et al. 2015; Phillips et al. 2019).

Data collection and processing

A sonde multiprobe (Hydrolab DS5X, Hach) was deployed near the center of Mývatn's south basin during the summer months (late May through late August) from 2012 to 2018. This location corresponded with a routine monitoring station

that was manually sampled approximately weekly during the periods of sonde deployment for standard water column variables (e.g., DO, light, and temperature) as well as benthic variables such as larval midge density and sediment chlorophyll. The sonde was attached to a buoy so that the sensors sat at a depth of 0.5 m. This location is quite shallow (3.3 m) and well mixed (including for oxygen concentrations; Supporting Information Fig. S9), such that the sensor measurements represent integrated values throughout the water column. The sonde measured temperature, DO, turbidity, and phycocyanin (a cyanobacterial pigment) every 30 min. However, DO data were unavailable from 2014 due to probe failures, so only 2012–2013 and 2015–2018 data were used in this analysis. The sensor data had occasional anomalies (usually associated with battery failures), which I removed by first excluding values that exceeded thresholds of plausibility (<5 mg L⁻¹ for DO and >18°C for temperature) based on weekly profiles at 0.5-m intervals taken with handheld probes (ProODO, YSI) or visual inspection (>200 V for turbidity). I then excluded values that deviated from the mean on a given day by more than two standard deviations (SDs). This resulted in the omission of 5.6% of the observations (Supporting Information Figs. S5 and S6). There were no indications of sensor drift (Supporting Information), and therefore no drift correction was applied. I averaged the half-hourly measurements to an hourly scale to match the resolution of the local weather data (solar irradiance and wind speed), which resulted in minimal loss of information due to the high temporal autocorrelation in the measurements (Supporting Information).

Light readings were taken either every 15 or 30 min (depending on the year) with a light/temperature logger (HOBO Pendant, Onset Computer Corporation) attached to the top of the buoy deploying the sonde; I averaged these data to an hourly scale for further analysis. However, HOBO logger data were missing in 2012, so I used downwelling solar irradiance from the local weather station, which were strongly correlated with the HOBO logger data ($r = 0.79$; Supporting Information). Solar irradiance was not available in 2018, so it would not have been possible to use the same metric for all 6 years of data. The HOBO logger (measured in lux) and solar irradiance (measured in watts) were converted to photosynthetically active radiation (PAR; measured in µmol-photons m⁻² s⁻¹) based on a standard relationship (Thimijan and Heins 1983). To estimate light below the water surface, I regressed the surface PAR estimates to PAR measurements taken approximately 5 cm below the water surface during routine monitoring using a Li-192 Quantum Underwater Sensor, Li-COR (Supporting Information). I used resulting regression equation to translate PAR from the HOBO logger and weather station into PAR below the water surface for each time point in the sonde data. While the HOBO logger and weather station light data are subject to some uncertainty (Long et al. 2012), they should nonetheless provide a reasonable characterization of major changes in light conditions.

While models of lake metabolism often use light levels at the water's surface, primary production occurs throughout the water column and in the benthos, and water column light levels are subject to large changes relative to surface light due to changes in water clarity (Obrador et al. 2014). Therefore, I estimated the mean light level throughout the water column given observed variation in surface light and water clarity as

$$\overline{L_{d,h}(z)} = \frac{1}{z_{\max}} \int_0^{z_{\max}} L_{d,h}^0 e^{-c_{d,h} z} dz = \frac{L_{d,h}^0 (1 - e^{-c_{d,h} z_{\max}})}{z_{\max} c_{d,h}}, \quad (1)$$

where z (m) is the vertical position in the water column, z_{\max} is the water column depth (3.3 m), $L_{d,h}^0$ is the PAR ($\mu\text{mol-photon m}^{-2} \text{s}^{-1}$) at the water surface ($z = 0$) and $c_{d,h}$ is the rate at which light attenuates through the water column. For simplicity, I henceforth denote $\overline{L_{d,h}(z)}$ as $L_{d,h}$. To estimate $c_{d,h}$, I regressed observed light attenuation calculated from weekly measurements of PAR at 0.5-m depth intervals against turbidity measured simultaneously by the sonde. I used this regression ($R^2 = 0.66$; Supporting Information Fig. S10) to predict $c_{d,h}$ from turbidity for each time point in the sonde data. While the mean water column light levels are more biologically relevant, they are also more uncertain than the estimates of surface light levels. Therefore, I performed the analysis using both sets of light levels, which yielded similar results. The results using mean water column light are presented in the main text, while results using surface light are shown in Supporting Information Figs. S17 and S18.

Model structure

The model is a modified version of the model presented by Holtgrieve et al. (2010), which characterizes changes in DO due to NEP with a saturating P-I curve (similar to Obrador et al. 2014; Staehr et al. 2016). However, rather than treating the parameters of the P-I curve as fixed over a given time period (requiring the model to be fit iteratively to obtain estimates of temporal variation in the P-I curve), the model presented here explicitly characterizes changes in the P-I curve utilizing data across all time periods (hourly measurements across six summers) simultaneously. This takes advantage of the fact that the physical and biological processes governing ecosystem metabolism and other aspects of DO dynamics are correlated through time, which means that this shared information can be used to inform the parameter estimates across all time points. Furthermore, this method is statistically unified because it uses all of the data to fit a single model, which facilitates characterizing the uncertainty in the estimates of temporally variable parameters of the P-I curve.

Table 1 defines all of the variables used in the model. Following Holtgrieve et al. (2010), $\text{NEP}_{d,h}$ in hour h on day d is decomposed into contributions from $\text{GPP}_{d,h}$ and $\text{ER}_{d,h}$ as

$$\text{NEP}_{d,h} = \text{GPP}_{d,h} - \text{ER}_{d,h}, \quad (2)$$

with all three components quantified as total change in oxygen throughout the water column, resulting in a flux per unit

area ($\text{mg O}_2 \text{ m}^{-2} \text{ h}^{-1}$), based on a mixing depth of 3.3 m. However, the data used to fit the model were only taken from a single sampling location, so these estimates are not assumed to characterize the metabolism across the entire lake as this would require spatially replicated DO measurements (Van de Bogert et al. 2007).

I modeled $\text{GPP}_{d,h}$ as a saturating function of average light throughout the water column $L_{d,h}$ ($\mu\text{mol-photon m}^{-2} \text{ s}^{-1}$):

$$\text{GPP}_{d,h} = \beta_{d,h} \tanh\left(\frac{\alpha_d}{\beta_{d,h}} L_{d,h}\right), \quad (3)$$

where $\beta_{d,h}$ ($\text{mg O}_2 \text{ m}^{-2} \text{ h}^{-1}$) is the maximum potential GPP ("max GPP"; Fig. 1) attained at high light levels and α_d ($\text{mg O}_2 \text{ s } \mu\text{mol-photon}^{-1} \text{ h}^{-1}$) is the rate at which GPP increases with $L_{d,h}$ when $L_{d,h}$ is near zero ("initial slope") (Jassby and Platt 1976; Holtgrieve et al. 2010).

While many models of lake metabolism assume that GPP is insensitive to temperature (including Holtgrieve et al. 2010), primary production tends to increase with temperature particularly when light is saturating (Demars et al. 2016; Edwards et al. 2016; Richardson et al. 2017). Therefore, I modeled the maximum potential GPP as

$$\beta_{d,h} = \beta_d^0 \gamma_\beta^{((T_{d,h} - T_0)/\Delta T)}, \quad (4)$$

where β_d^0 is the maximum potential GPP on a given day at the mean water temperature for the entire time series T_0 (12°C), $T_{d,h}$ is the observed water temperature, and $\Delta T = 1^\circ\text{C}$ to make the exponent dimensionless. The parameter γ_β (dimensionless) describes the scaling of $\beta_{d,h}$ with changes in temperature. For example, if $\gamma_\beta = 1.2$, then a 1°C increase in $T_{d,h}$ above the mean temperature would result in a 20% increase in $\beta_{d,h}$. This approach follows the equation used by Venkiteswaran et al. (2007) for temperature dependence of respiration and is mathematically similar to the Arrhenius equation that has previously been used to model the relationship between ecosystem metabolism and temperature based on enzyme kinetics (Demars et al. 2016; Schindler et al. 2017). I opted for this alternative parameterization as it is simpler and does not require interpretation in terms of enzyme kinetics. While γ_β could in principle vary through time, temporal variation in the response of GPP to temperature is partially captured by variation in β_d^0 . Therefore, for greater tractability γ_β is fixed across all time points.

Daily changes in maximum GPP not due to temperature (e.g., changes in primary producer biomass or biomass-specific photosynthetic rates) were described by changes in β_d^0 , which I modeled as a multiplicative stochastic process analogous to exponential population growth:

$$\begin{aligned} \beta_d^0 &= \beta_{d-1}^0 e^{\delta_{d-1}^\beta}, \\ \delta_d^\beta &\sim \mathcal{N}(0, \sigma_\beta), \end{aligned} \quad (5)$$

Table 1. Definition of variables used in the model.

Variables	Description	Units	Timescale	Source
$DO_{d,h}^{obs}$	Observed DO	$mg\ O_2\ m^{-3}$	Hourly	Observed data
$DO_{d,h}^{eq}$	Equilibrium DO	$mg\ O_2\ m^{-3}$	Hourly	Observed data
$L_{d,h}$	Mean water column light	$\mu mol\ photons^{-1}\ s^{-1}$	Hourly	Observed data*
$T_{d,h}$	Water temperature	$^{\circ}C$	Hourly	Observed data
T_0	Reference temperature	$^{\circ}C$	Fixed	Observed data [†]
$\omega_{d,h}$	Wind speed	$m\ s^{-1}$	Hourly	Observed data
Z_{mix}	Mixing depth	m	Hourly	Observed data
$k_{d,h}$	Piston velocity	$m\ h^{-1}$	Fixed	Literature [‡]
$NEP_{d,h}$	Net ecosystem production	$mg\ O_2\ m^{-2}\ h^{-1}$	Hourly	Model fit
$GPP_{d,h}$	Gross primary production	$mg\ O_2\ m^{-2}\ h^{-1}$	Hourly	Model fit
$ER_{d,h}$	Ecosystem respiration	$mg\ O_2\ m^{-2}\ h^{-1}$	Hourly	Model fit
$EXC_{d,h}$	Oxygen flux to air	$mg\ O_2\ m^{-2}\ h^{-1}$	Hourly	Model fit
$DO_{d,h}$	Modeled DO	$mg\ O_2\ m^{-3}$	Hourly	Model fit
$\beta_{d,h}$	Max GPP (including temp)	$mg\ O_2\ m^{-2}\ h^{-1}$	Hourly	Model fit
β_d^0	Max GPP	$mg\ O_2\ m^{-2}\ h^{-1}$	Daily	Model fit
α_d	Initial slope of P-I curve	$mg\ O_2\ s\ \mu mol\ photons^{-1}\ h^{-1}$	Daily	Model fit
ρ_d	Baseline ER	$mg\ O_2\ m^{-2}\ h^{-1}$	Daily	Model fit
γ_{β}	Scaling of GPP with temperature	Dimensionless	Fixed	Model fit
γ_{ρ}	Scaling of ER with temperature	Dimensionless	Fixed	Model fit
σ_{β}	SD of change in β_d^0	Dimensionless	Fixed	Model fit
σ_{α}	SD of change in α_d	Dimensionless	Fixed	Model fit
σ_{ρ}	SD of changes in ρ_d	Dimensionless	Fixed	Model fit
σ_{proc}	Process error SD	$mg\ O_2\ m^{-3}$	Fixed	Model fit
σ_{obs}	Observation error SD	$mg\ O_2\ m^{-3}$	Fixed	Model fit

DO, dissolved oxygen; ER, ecosystem respiration; GPP, gross primary production; NEP, net ecosystem production; P-I, photosynthesis-irradiance; SD, standard deviation.

*Calculated from observed surface light and light attenuation estimated from turbidity.

[†]Defined as 12°C, based on observed mean water temperature in the dataset.

[‡](Cole and Caraco 1998).

where δ_d^{β} is the daily the rate of change in β_d^0 with SD σ_{β} . This is equivalent to modeling β_d^0 as a random walk on a log scale; this ensures that β_d^0 remains positive (negative values are biologically unintelligible). The stochastic process implies temporal autocorrelation in the estimates of β_d^0 , which has the consequence of smoothing the estimates through time with the degree of smoothing being influenced by the observed data (Zeng et al. 1998; Ives and Dakos 2012). Analogously, I modeled daily variation in the initial slope of the P-I curve α_d as

$$\begin{aligned}\alpha_d &= \alpha_{d-1} e^{\delta_d^{\alpha}}, \\ \delta_d^{\alpha} &\sim \mathcal{N}(0, \sigma_{\alpha}),\end{aligned}\quad (6)$$

with the rate of change δ_d^{α} and SD σ_{α} .

Daily and hourly variation in ER was modeled as a function of temperature:

$$ER_{d,h} = \rho_d \gamma_{\rho}^{((T_{d,h} - T_0)/\Delta T)}, \quad (7)$$

where ρ_d ($mg\ O_2\ m^{-2}\ h^{-1}$) is the baseline respiration rate at T_0 and γ_{ρ} (dimensionless) is the temperature scaling of ER_d (Holtgrieve et al. 2010). Similar to β_d^0 and α_d , daily variation in ρ_d (e.g., changes in biomass or biomass-specific respiration of all aerobic organisms) was modeled as

$$\begin{aligned}\rho_d &= \rho_{d-1} e^{\delta_d^{\rho}}, \\ \delta_d^{\rho} &\sim \mathcal{N}(0, \sigma_{\rho}),\end{aligned}\quad (8)$$

with the rate of change δ_d^{ρ} and SD σ_{ρ} . Various studies have documented diel variation in ER with response to factors other than temperature (Sadro et al. 2011), and these have occasionally been incorporated into models of lake ecosystem metabolism (e.g., Schindler et al. 2017). However, the primary goal of the present analysis was to estimate variation in ecosystem metabolism rates between days, and it is likely that incorporating diel variation in respiration not due to temperature would have a minimal impact on the estimates of daily variation (Hanson et al. 2008). Therefore, to reduce the complexity of

the model, I did not include diel variation in ER driven by factors other than temperature.

I estimated parameters for Eqs. 2–8 from the observed DO time series by modeling the hourly concentration of DO ($\text{mg O}_2 \text{ m}^{-3}$) as

$$\text{DO}_{d,h} = \text{DO}_{d,h-1} + \frac{\Delta h (\text{NEP}_{d,h-1} + \text{EXC}_{d,h-1})}{z_{\text{mix}}} + \epsilon_{d,h-1}^{\text{proc}} \quad (9)$$

where $\Delta h = 1 \text{ h}$, $\text{EXC}_{d,h}$ ($\text{mg O}_2 \text{ m}^{-2} \text{ h}^{-1}$) is the exchange of oxygen between the water and the air, z_{mix} is the mixing depth (3.3 m), and $\epsilon_{d,h-1}^{\text{proc}}$ is the processes error, defined as

$$\epsilon_{d,h}^{\text{proc}} \sim \mathcal{N}(0, \sigma_{\text{proc}}), \quad (10)$$

where σ_{proc} is the SD of the stochastic changes in DO (see below for description of the observation model linking Eq. 9 to the observed data).

$\text{EXC}_{d,h}$ is the oxygen flux across the air–water boundary, defined with respect to the water (i.e., a negative flux corresponds to a loss of O_2 from the water):

$$\text{EXC}_{d,h} = k_{d,h} (\text{DO}_{d,h}^{\text{eq}} - \text{DO}_{d,h}), \quad (11)$$

where $\text{DO}_{d,h}^{\text{eq}}$ is the atmospheric equilibrium (i.e., saturation) concentration of oxygen based on temperature, pressure, and salinity (Staehr et al. 2010a). The parameter $k_{d,h}$ is known as the “piston velocity” and scales the rate of gas exchange across the air–water boundary. The parameterization of $k_{d,h}$ is subject to much uncertainty and can have a large influence on metabolism estimates (Dugan et al. 2016). Here, I employed the widely used parameterization of Cole and Caraco (1998):

$$k_{d,h} = \left(k_0^{600} + k_1^{600} \omega_{d,h}^{k_2^{600}} \right) \left(\frac{\text{Sc}_{\text{O}_2}(T_{d,h}, S)}{600} \right)^{-0.5}, \quad (12)$$

where $\omega_{d,h}$ is the wind speed (m s^{-1}), $k_0^{600} = 2.07$, $k_1^{600} = 0.215$, and $k_2^{600} = 1.7$, and $\text{Sc}_{\text{O}_2}(T_{d,h}, S)$ is the Schmidt number for oxygen at the observed temperature and salinity (the values of k_0^{600} and k_1^{600} give $k_{d,h}$ in units of cm h^{-1} , which I then converted to m h^{-1}). However, to explore the sensitivity of the metabolism estimates to the parameterization of $k_{d,h}$ I also fit the model using the parameterization of Crusius and Wanninkhof (2003), which has the same functional form as Eq. 12 but uses different values of the constants ($k_0^{600} = 0.168$, $k_1^{600} = 0.228$, and $k_2^{600} = 2.2$) and overall has much greater sensitivity to wind speed than the parameterization of Cole and Caraco (1998). The two parameterizations for $k_{d,h}$ gave very similar inferences for ecosystem metabolism, likely because of the ability of the process errors $\epsilon_{d,h}^{\text{proc}}$ to absorb variability not readily

attributable to biological processes, such as not fully characterizing exchange with the atmosphere. Therefore, the results using the Cole and Caraco (1998) parameterization are presented in the main text, while the results using Crusius and Wanninkhof (2003) are reported in Supporting Information Figs. S14–S16.

It is important to note that Eq. 9 does not strictly follow mass balance; because $\text{ER}_{d,h}$ is not a function of oxygen concentration, theoretically, it can exceed the amount of available oxygen. In most applications (including here), oxygen concentrations are sufficiently high that respiration is not oxygen limited. However, the potential for negative values to arise during model fitting influences the choice of appropriate descriptions of process and observation error. For example, using a lognormal error model might fail because it could require taking the log of negative predicted values. I used the most straightforward approach (as in other studies) of assuming Gaussian process and observation error, relying on the data to guide the model to physically meaningful values. This yielded the following observation equation:

$$\text{DO}_{d,h}^{\text{obs}} = \text{DO}_{d,h} + \epsilon_{d,h}^{\text{obs}}, \quad (13)$$

where $\epsilon_{d,h}^{\text{obs}}$ is the observation error, modeled as

$$\epsilon_{d,h}^{\text{obs}} \sim \mathcal{N}(0, \sigma_{\text{obs}}), \quad (14)$$

where σ_{obs} is the SD of the observation process. The central statistical difference between the process and observation errors is that process errors propagate through time and manifest as relatively smooth variations, while observation errors do not propagate and appear “noisy” (Box et al. 1994).

Model fitting

Observed DO time series were fit to all 6 years (2012–2013 and 2015–2018) simultaneously. The initial values for continuous stretches of hourly observations (i.e., without missing data or spanning years) were modeled based on Eqs. 13 and 14, with the mean of the Gaussian distribution set to the observed value for that time step. The presence of missing values meant that some continuous series had a small number of observations. While in principle, the model could accommodate these short series because the parameters’ estimates would be informed by the longer series, the short series likely contributed little meaningful information. Therefore, I removed any continuous series with fewer than 24 observations (i.e., 1 d worth of observations). A single continuous stochastic process was used to model β_d^0 , α_d , and ρ_d for each year (specified by Eqs. 5, 6, and 8, respectively), with the model “skipping” over unobserved days (37 out of 382 d).

I fit the model with a Bayesian approach via Stan 2.17.0 run from R 3.5.1 (R Core Team 2018) using the ‘rstan’ package (Stan Development Team 2018). Stan uses Hamiltonian Monte

Carlo to generate Markov chains that converge to a stationary distribution approximating the joint posterior distribution for the unobserved variables (Carpenter et al. 2017). I centered the observed DO on its mean and divided by its SD across all time points and then scaled the model parameters accordingly (Supporting Information). Scaling the model stabilized the fitting process and also facilitated the use of Gaussian distributions on unit scale as weakly informative priors (SD of 1 and truncated at 0 or 1 for those parameters with corresponding lower bounds; see Supporting Information for further details). I used four independent chains with diffuse initial values and 2000 iterations including a 1000-iteration “warm-up.” Convergence was assessed by examining trace plots for parameter estimates and the potential-scale reduction factor (\hat{R}), which quantified the relative variance within and between chains to determine whether stationarity was achieved (values near 1 indicate convergence; see Supporting Information for detailed specifications for the fitting routine and additional diagnostics).

Attempting to estimate both σ_{obs} and σ_{proc} independently resulted in very inefficient sampling of the posterior distribution as σ_{obs} slowly approached 0 (Supporting Information Fig. S11). Therefore, I fit the model with σ_{obs} set to 1% of the observed SD in DO (which was computationally more convenient than setting it to exactly 0). This resulted in much more efficient sampling and estimates for model parameters that were similar to the model with σ_{obs} estimated independently (Supporting Information Fig. S12). It was not surprising that σ_{obs} was low, as the observed time series of DO (filtered for anomalous values) lacked the appearance of high-frequency noise that would be indicative of observation error (Supporting Information Fig. S13). This is partially due to the fact that I used hourly data that were averaged from half-hourly data; observation error would likely have been more substantial for higher frequency data.

The posteriors for all parameters were unimodal and at most only modestly skewed, justifying the use of quantiles to provide summaries for parameter estimates. Throughout I use posterior medians for point estimates and 16% and 84% quantiles for the bounds of 68% uncertainty intervals (“ui_{68%}”) to match the coverage of standard errors. I expressed values for total daily values for GPP, ER, and NEP in units $\text{g O}_2 \text{ m}^{-2} \text{ d}^{-1}$ rather than $\text{mg O}_2 \text{ m}^{-2} \text{ h}^{-1}$ to facilitate a more natural comparison to other reported values for ecosystem metabolism in both aquatic and terrestrial systems.

Model comparison

The full version of the model estimated different values for the parameters of the P-I curve (β_d^0 , α_d , and ρ_d) for each day. To determine whether the inferred changes in the P-I curve were actually supported by the data, I fit a simplified version of the model with the parameters of the P-I curve fixed through time (equivalent to setting σ_β , σ_α , and σ_ρ to 0). In this simplified model, temporal changes in ecosystem metabolism were due entirely to light and temperature. I then compared the fit of

the two models using the Leave-One-Out Information Criterion (LOOIC), which is related to widely applicable information criterion used in some previous studies of lake metabolism (e.g., Schindler et al. 2017) but has been shown to be more robust (Vehtari et al. 2017). LOOIC is conceptually similar to likelihood-based information criteria (e.g., Akaike information criterion and Bayesian information criterion), and it is reported in units of deviance so that it can be interpreted in a similar manner. I calculated LOOIC using the “loo” package in R 3.5.1 (R Core Team 2018).

Variance partitioning

I partitioned variance in GPP, ER, and NEP into contributions from light, temperature, and the time-varying parameters using the “delta method” (Clark 2007). This approach differs from a more conventional partitioning (e.g., ANOVA) by explicitly accounting for nonlinearities and covariances between variables. The delta method is a locally linear approximation of the variance relative to the mean values of the input variables (see Supporting Information for a full mathematical description). In general, the contribution of a parameter (e.g., temperature) to the variance in a function of that parameter (e.g., GPP) is determined by (1) the sensitivity of the function to changes in the parameter and (2) the overall variability of that parameter. For example, temperature could explain a large portion of the variance in GPP either because (1) GPP is very sensitive to temperature or (2) because temperature itself has a high variance. For each variable, I report the squared coefficient of variation (CV^2) and “scaled sensitivity” (as defined in Supporting Information Eqs. S16 and S17), with the latter including the effect of correlations between variables. The product of CV^2 and scaled sensitivity equals the relative contribution of a given variable to the variance in the response (Supporting Information Eq. S17).

Drivers of maximum GPP

To explore the possible drivers of variation in maximum GPP (which was the dominant contributor to variation in lake metabolism, see Results), I fit linear models regressing β_d^0 against daily mean phycocyanin concentration (as a measure of cyanobacterial abundance; comparable data for other photosynthetic pigments were not available) and larval midge abundance, which has previously shown to have large effects on Mývatn’s benthic production (Herren et al. 2017; Phillips et al. 2019). Phycocyanin data were collected by the sonde and were available for all days for which there were estimates of β_d^0 . The midge larvae data were collected approximately weekly from the central sampling station from sediment cores (Kajak corer; 0.5 m length and 5 cm diameter), which were sieved through either $63 \mu\text{m}$ (top 5 cm) or $125 \mu\text{m}$ (remaining sediment) mesh to collect the larva.

Because the phycocyanin data were available daily, while the midge data were only available weekly, I fit two models: (1) including phycocyanin for all days, and (2) including both

phycocyanin and midge abundance for those days when midge samples were collected. For midge abundance, I used total counts of the two dominant midge taxa previously shown to have positive effects on benthic primary production (*Tanytarsus gracilentus* and *Chironomus islandicus*) (Herren et al. 2017; Phillips et al. 2019) averaged across replicated samples for a given date. I z-transformed (subtracted the mean and divided by the SD across all time points) all variables and included an autoregressive correlation structure grouped by year to account for temporal autocorrelation in estimates of β_d^0 (Pinheiro et al. 2018).

Data and code availability

Data and code can be found at https://github.com/jsphillips2/sonde_oxygen.

Results

Ecosystem metabolism rates

Mean daily estimates of GPP ($5.34 \text{ g O}_2 \text{ m}^{-2} \text{ d}^{-1}$; $ui_{68\%} = [5.20, 5.49]$) and ER ($4.63 \text{ g O}_2 \text{ m}^{-2} \text{ d}^{-1}$; $ui_{68\%} = [4.46, 4.79]$) were large overall, reflecting Mývatn's eutrophic state. Both showed substantial variation through time, both within and between years (Fig. 2). However, because GPP and ER were correlated (Pearson correlation = 0.75; $df = 343$; $p < 0.001$; Fig. 3), NEP remained comparatively stable and slightly above zero ($0.72 \text{ g O}_2 \text{ m}^{-2} \text{ d}^{-1}$; $ui_{68\%} = [0.64, 0.80]$). This indicates that Mývatn was net autotrophic during the summer months over this time period. Overall, the high ecosystem metabolism rates accounted for approximately 21% of the total variation in

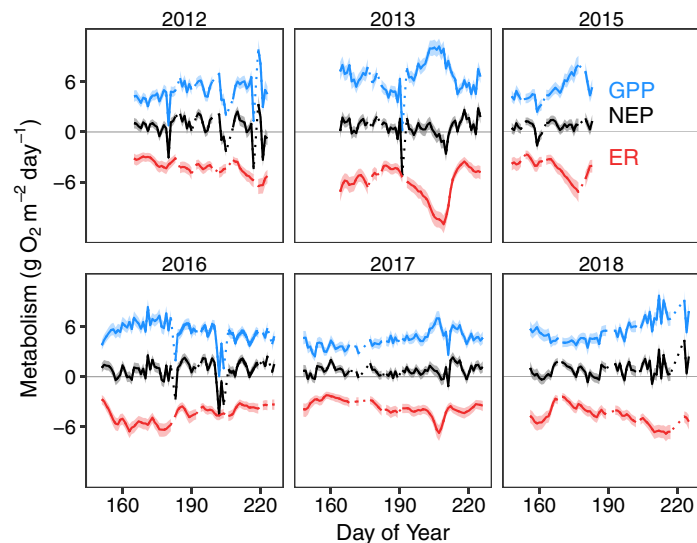


Fig. 2. Daily estimates of GPP, ER, and NEP, plotted through time. Metabolism rates are expressed as changes in water column DO (e.g., ER is negative because it reduces DO). The lines are the posterior medians, and the shaded regions are the 68% uncertainty intervals matching the coverage of standard errors. [Color figure can be viewed at wileyonlinelibrary.com]

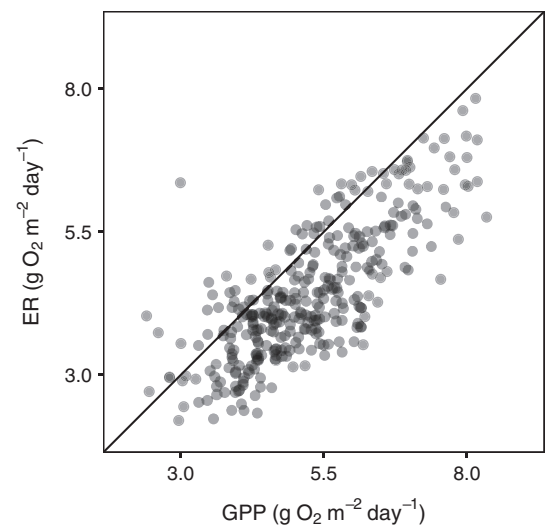


Fig. 3. Estimated daily ER plotted against GPP, with the one-to-one line. The estimates of ER and GPP include the influence of temperature, which contributes to their correlation.

observed hourly DO (obtained through variance partitioning by applying Supporting Information Eq. S14 to main text Eq. 9).

Temperature-sensitivity of GPP and ER

ER was very sensitive to temperature, with $\gamma_p = 1.15$ implying that 1°C increase (or decrease) from the reference temperature would result in a 15% increase (or 13% decrease) in ER. GPP was also sensitive to temperature ($\gamma_p = 1.06$), although substantially less so than ER.

Time-varying parameters of the P-I curve

The metabolism parameters β_d^0 , α_d , and ρ_d all substantially varied through time, with the SDs of their associated stochastic processes clearly different from 0 (Table 2; Figs. 4 and 5). Furthermore, comparison of the full model to a reduced model with the metabolism parameters fixed through time indicated strong support for the full model ($\Delta\text{LOOIC} = 31.2$; in units of deviance as for ΔAIC). Together, these results indicate that there was statistically meaningful temporal variation in Mývatn's P-I curve. The initial slope of the P-I curve (α_d) was by far the most temporally variable parameter, with an approximately 15-fold difference between minimum and maximum values (Fig. 4). This indicates that the response of GPP to variation in light under light-limiting conditions was very dynamic. Several years showed similar seasonal patterns, with α_d starting low and increasing to a peak midsummer, followed by a steep decline. However, in 2012 and 2016 α_d declined gradually throughout the season.

Maximum GPP (β_d^0) was the next most variable parameter of the P-I curve (3.5-fold variation between minimum and maximum values; Fig. 5) and displayed consistent seasonal patterns, with steady increases from early to midsummer followed

Table 2. Posterior summaries of fixed (not time-varying) parameters, using posterior medians as point estimates and 16% and 84% quantiles as bounds of 68% uncertainty intervals (“ $ui_{68\%}$ ”) to match the coverage of standard errors.

Parameters	Description	Estimate* [$ui_{68\%}$]
γ_β	Scaling of GPP with temperature	1.06 [1.05, 1.08]
γ_ρ	Scaling of ER with temperature	1.15 [1.13, 1.18]
$\bar{\beta}_d^0$	Maximum GPP (median across all days)	368 [326, 414]
$\bar{\alpha}_d$	Initial slope of P-I curve (median across all days)	5.44 [3.74, 8.06]
$\bar{\rho}_d$	Baseline ER (median across all days)	156 [133, 181]
σ_β	SD of change in β_d^0	0.06 [0.05, 0.07]
σ_α	SD of change in $\alpha_{d,h}$	0.21 [0.18, 0.25]
σ_ρ	SD of changes in ρ_d	0.05 [0.04, 0.08]
σ_{proc}	Process error SD	0.099 [0.098, 0.101]

DO, dissolved oxygen; ER, ecosystem respiration; GPP, gross primary production; NEP, net ecosystem production; P-I, photosynthesis-irradiance; SD, standard deviation.

*The estimates for σ_{proc} are expressed in terms of the SD of the observed DO data. All other parameters are in units as defined in Table 1.

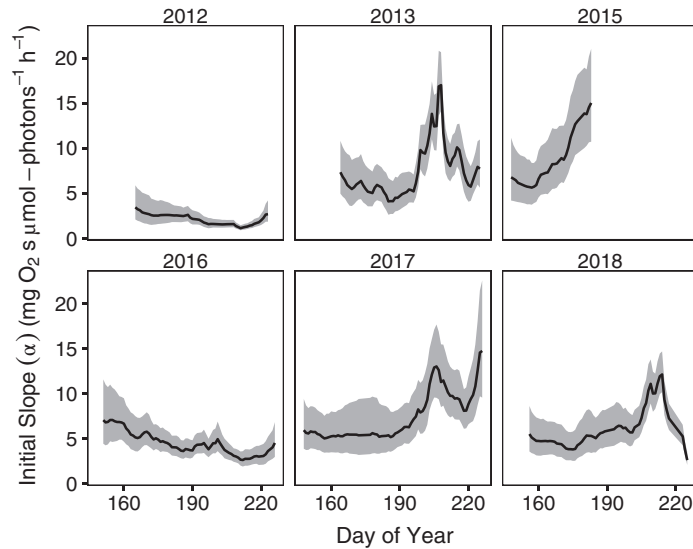


Fig. 4. Initial slope of the P-I curve as inferred from the model, plotted through time. The lines are the posterior medians, and the shaded regions are the 68% uncertainty intervals matching the coverage of standard errors.

by a plateau or a modest decline. Baseline ER (ρ_d) was the least variable parameter, with only 2.5-fold variation (Fig. 5). Maximum GPP and baseline ER were only modestly correlated across all time points (Pearson correlation = 0.51 across all years; $df = 343$; $p < 0.001$), and in some years their associations were only weakly positive or even negative (Fig. 6). This means that apparent coupling between overall GPP and ER rates (Fig. 3) is due in part to the shared responses to temperature,

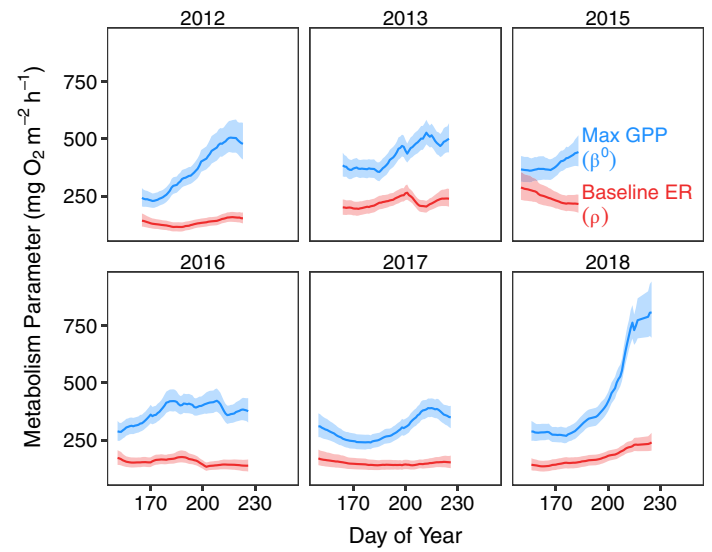


Fig. 5. Maximum GPP and baseline ER (at the reference temperature of 12°C) as inferred from the model, plotted through time. The lines are the posterior medians, and the shaded regions are the 68% uncertainty intervals matching the coverage of standard errors. [Color figure can be viewed at wileyonlinelibrary.com]

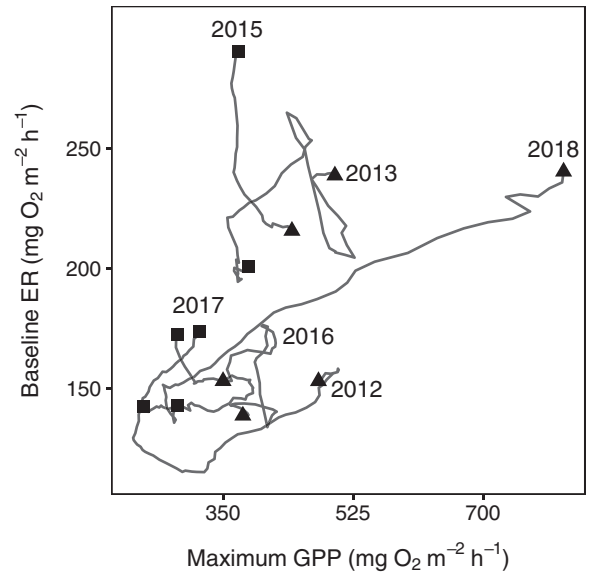


Fig. 6. Baseline ER plotted against maximum GPP, both defined at the reference temperature of 12°C. Each line represents a separate year, with squares indicating the beginning and triangles the end of each series.

rather than being solely due to temporal changes in the parameters of the P-I curve (i.e., maximum GPP and baseline ER).

The parameters of the P-I curve were estimated using the average light throughout the water column, which varied due to changes in both surface light and to water clarity. To explore the importance of variation in water clarity, I also fit the model using surface light and compared the resulting parameter estimates to those using the average water column

light (as above). The estimates of baseline ER and maximum GPP were largely the same, as they should be given that they characterize metabolism when light is 0 (i.e., when surface and water column light are the same) and when light is saturating (i.e., when differences between surface and water column later are irrelevant) (Supporting Information Fig. S17). The average value of the initial slope of the P-I curve was substantially lower for the model fit using surface light, which again was as expected because the surface light values were always higher than the water column values (Supporting Information Fig. S18). However, the temporal patterns were very similar, with the largest differences being relatively high values in 2015 and 2018 when using the water column light. These 2 years had substantial declines in water column light due to reduced water clarity associated with cyanobacterial blooms, which suggests that the initial slope of the P-I curve partially compensated for the declines in water clarity. This is consistent with the fact that the initial slope was negatively correlated with the average water column light levels (Pearson correlation = -0.44 ; $df = 236$; $p < 0.001$).

Variance partitioning

Most of the variation in GPP was due to variation in the maximum GPP, with temperature as the second most important contributor (Table 3). In contrast, the contributions of variation in light and the initial slope of the P-I curve were quite small, despite the fact that these two variables had comparatively high coefficients of variation. This is because GPP was relatively insensitive to changes in these variables, due to the average light level

($144 \mu\text{mol-photon m}^{-2} \text{ s}^{-1}$) generally being in the saturated part of the P-I curve. Furthermore, the initial slope of the P-I curve and average water column light were negatively correlated with each other (Pearson correlation = -0.44 ; $df = 236$; $p < 0.001$), and this negative correlation reduced the contribution of both variables to temporal variation in GPP (following Supporting Information Eq. S15). Variation in baseline ER and temperature made comparable contributions to variance in ER, owing to their similar variability and sensitivities. Note that the variance partitioning is an approximation around the means of the input variables (i.e., light, temperature, and time-varying parameters) and so reflects the contribution of variation in different variables centered around the average conditions.

Because GPP and ER had opposite effects on NEP, variables with correlated effects on GPP and ER had reduced contributions to the variance in NEP. Consequently, both temperature (positively related to both GPP and ER) and the baseline ER (correlated with maximum GPP) had negligible or even slightly negative contributions. The contribution of variation in light was slightly higher for NEP than for GPP, while the contribution of variation in the initial slope was slightly lower. Maximum GPP was by far the largest contributor to variation in NEP, with a relative contribution of 0.89 despite being correlated with baseline ER. This is because the sensitivity of NEP to maximum GPP was substantially higher than its sensitivity to baseline ER.

Drivers of maximum GPP

Maximum GPP at high light (β_d^0) was quite variable and was the dominant contributor to variation in overall GPP and

Table 3. Variance partitioning of GPP, ER, and NEP into contributions from light, temperature, and the time-varying parameters of the P-I curve. The CV^2 and scaled sensitivity are dimensionless and can therefore be compared for different variables. The relative contribution to the variance equals the product of the CV^2 and scaled sensitivity.

	CV^2 [ui _{68%}]	Scaled sensitivity [ui _{68%}]	Relative contribution to variance [ui _{68%}]
GPP			
Initial slope	0.38 [0.30, 0.48]	0.09 [0.04, 0.15]	0.04 [0.02, 0.06]
Maximum GPP	0.09 [0.07, 0.11]	7.95 [6.69, 9.63]	0.71 [0.63, 0.78]
Temperature	0.03*	5.81 [3.72, 7.97]	0.17 [0.11, 0.23]
Light	1.67*	0.05 [0.02, 0.8]	0.08 [0.04, 0.13]
ER			
Baseline ER	0.08 [0.05, 0.11]	5.56 [3.96, 7.44]	0.44 [0.32, 0.58]
Temperature	0.03*	19.10 [14.7, 23.2]	0.56 [0.42, 0.68]
NEP			
Initial slope	0.38 [0.30, 0.48]	0.06 [0.00, 0.13]	0.02 [0.00, 0.05]
Max GPP	0.09 [0.07, 0.11]	10.10 [8.44, 12.2]	0.89 [0.79, 0.99]
Baseline ER	0.08 [0.05, 0.11]	-0.41 [-1.40, 0.373]	-0.03 [†] [-0.09, 0.04]
Temperature	0.03*	-0.79 [-1.70, 0.13]	-0.02 [†] [-0.05, 0.00]
Light	1.67*	0.08 [0.04, 0.13]	0.13 [0.07, 0.22]

DO, dissolved oxygen; ER, ecosystem respiration; GPP, gross primary production; NEP, net ecosystem production; P-I, photosynthesis-irradiance; SD, standard deviation.

*The environmental variables are inputs to the model and therefore have no modeled uncertainty in their coefficients of variation.

[†]Negative contributions to variance in metabolism arise due to covariances with other parameters, resulting in compensatory effects on metabolism.

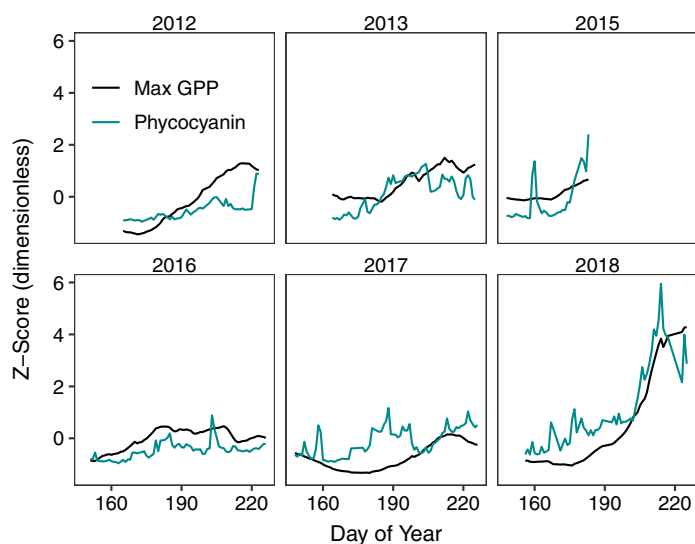


Fig. 7. Maximum GPP inferred from the model and phycocyanin concentration (a cyanobacterial pigment), plotted through time. Both variables are shown as z-scores (centered on mean and divided by SD across all days). [Color figure can be viewed at wileyonlinelibrary.com]

NEP. Maximum GPP was positively related to phycocyanin in both the model for all observations ($df = 343$; $t = 3.65$; $p < 0.001$) (Fig. 7) and the model for days with midge samples ($df = 39$; $t = 2.87$; $p = 0.0066$) (Supporting Information Fig. S19). In contrast, there was no relationship between maximum GPP and midge abundance ($df = 39$; $t = -0.20$; $p = 0.84$) (Supporting Information Fig. S19). This suggests that increases in cyanobacterial abundance during blooms increased the maximum GPP, while midges had no effect.

Discussion

In this study, I used time series of DO from Lake Mývatn to estimate temporal variation in P-I curves and ecosystem metabolism across six summers. To do so, I employed a new approach that extended previous methods (Holtgrieve et al. 2010; Obrador et al. 2014; Staehr et al. 2016) by explicitly modeling temporal variation in the parameters governing ecosystem metabolism, taking advantage of the shared information across the full set of data. All of the parameters of the P-I curve (maximum GPP, initial slope of the P-I curve, and baseline ER) varied substantially through time, with the initial slope being particularly variable. However, variation in the maximum GPP made the largest contribution to variation in estimated NEP with respect to average conditions, with this variation being associated with increases in the abundance of cyanobacteria during blooms. Overall, these results illustrate how changes in the P-I curve can contribute substantially to temporal variation in lake ecosystem metabolism.

The dependence of photosynthesis on light is a major feature of most model-based studies of lake metabolism, either in the form of linear relationships (e.g., Batt and Carpenter 2012;

Solomon et al. 2013; Richardson et al. 2017) or nonlinear P-I curves (e.g., Holtgrieve et al. 2010; Obrador et al. 2014; Staehr et al. 2016; Schindler et al. 2017). However, in previous applications the main function of P-I relationships has been to partition NEP into contributions from GPP and ER (but see Holtgrieve and Schindler 2011; Staehr et al. 2016), which are then used as the main response variables in subsequent analyses to identify drivers of metabolism (e.g., Coloso et al. 2011; Solomon et al. 2013). In contrast, the present study places emphasis on the P-I curve itself, which helps to clarify the temporal patterns driven by physical and biological processes other than light and temperature (Staehr et al. 2016). For example, the maximum GPP can be understood as the overall photosynthetic potential of the ecosystem (Jassby and Platt 1976; Behrenfeld and Falkowski 1997) that is directly connected to drivers such as primary producer biomass or nutrient limitation. In Mývatn, variation in maximum GPP was the dominant contributor to the total variance in net metabolism and was primarily driven by episodic cyanobacterial blooms, a phenomenon which may be important in many of the world's lakes given the increasing prevalence of blooms (Taranu et al. 2015). In more oligotrophic systems, it is possible that the parameters of the P-I curve are less variable, which could mean that the relative contribution of light and temperature to temporal variation would be greater than observed in the relatively eutrophic Mývatn (Staehr et al. 2016).

The initial slope of the P-I curve has been suggested a crucial parameter for understanding lake metabolism (Holtgrieve and Schindler 2011; Staehr et al. 2016). In Mývatn, the initial slope was the by far the most temporally variable parameter of the P-I curve with 15-fold variation between its minimum and maximum values. However, despite its large variation, the initial slope of the P-I curve made only a small contribution temporal variation in lake metabolism. This was for two reasons. First, photosynthesis was largely saturated at the mean water column light level of $144 \mu\text{mol-photon m}^{-2} \text{ s}^{-1}$, such that changes in the initial slope were irrelevant. Average water column light levels are generally high in Mývatn because it is shallow and has clear water in the absence of blooms. However, in the deeper or more turbid lakes that are chronically light limited, it is likely that variation in the initial slope of the P-I curve would be more important for net ecosystem metabolism (Staehr et al. 2016). Second, changes in the initial slope were negatively correlated with variation in light, implying compensatory changes in the response to light that stabilized net metabolism. Photosynthetic organisms are very sensitive to light conditions and can increase their production of photosynthetic pigments with response to chronic light limitation, which in turn increases their sensitivity to low light levels (Falkowski 1984; Moore et al. 2006; Dubinsky and Stambler 2009). Furthermore, many phytoplanktons have the ability to change their position in the water column, which could increase their effective access to light and thereby increase the apparent sensitivity of the P-I curve to average

light conditions throughout the water column (Klausmeier and Litchman 2001). While compensatory changes in the light-sensitivity of ecosystem metabolism in response to seasonal light limitation have been previously observed (e.g., benthic communities in Greenland fjords; Attard et al. 2014), the general prevalence of this phenomenon for other aquatic systems is largely unknown and worthy of further study.

Many studies have considered the coupling of GPP and ER, because the balance between these two processes determines whether a given ecosystem is a net carbon source (“heterotrophic”) or sink (“autotrophic”). Systems dominated by autochthonous carbon are expected to have a strong coupling between GPP and ER, due both to respiration by photosynthetic organisms themselves and heterotrophic respiration of the organic carbon fixed through primary production (Del Giorgio et al. 1999; Solomon et al. 2013; Richardson et al. 2017; Schindler et al. 2017). Recent work has also suggested that correlated responses to temperature can couple GPP and ER (Solomon et al. 2013; Demars et al. 2016; Richardson et al. 2017), and distinguishing between these two mechanisms is important for predicting the response of GPP-ER coupling to long-term change (e.g., climate). In Mývatn GPP and ER were strongly correlated, and this was due to both temperature (to which both GPP and ER were sensitive) and correlations between the time-varying ecosystem metabolism rates (maximum GPP and baseline ER, controlling for temperature). Even though ER was more sensitive to temperature than GPP relative to its overall scale (i.e. $\gamma_\rho > \gamma_\beta$), the magnitude of GPP was much greater; consequently, the temperature-driven variations in ER and GPP largely negated each other in the resulting NEP. This suggests that net carbon flux from Mývatn is relatively insensitive changes in temperature. In contrast, the coupling between maximum potential GPP and baseline ER was only modestly positively ($R = 0.51$), allowing variation in maximum GPP to have a large effect on NEP. Given that Mývatn likely has low allochthonous inputs (being surrounded by low-productivity tundra; Gratton et al. 2008), it is surprising that the temperature-independent coupling of GPP and ER is not stronger. Solomon et al. (2013) argue that ER-GPP coupling should be weaker in eutrophic lakes when ER is substantially lower than GPP. However, Mývatn does not fit this pattern as overall ER during the most productive summer months was 86% of GPP. The unexpected decoupling of ER and GPP could be due to the high organic content of the lake sediment (itself the source of past primary production; Einarsson et al. 2004), which could fuel high respiration during periods of low GPP.

The relative contribution of benthic and pelagic organisms to primary production is of growing interest given the role of eutrophication in stimulating phytoplankton blooms, often at the expense of benthic production (Vadeboncoeur et al. 2002, 2003; Karlsson et al. 2009; Taranu et al. 2015). While many lakes are sufficiently deep and poorly mixed to have large

gradients in DO with depth (Obrador et al. 2014), in Mývatn the water column is sufficiently well mixed for a single DO sensor to detect signals of both pelagic and benthic production. Mývatn is generally regarded as being dominated by benthic production (Jónasson 1979; Einarsson et al. 2004), which is typical of shallow lakes that have large amounts light reaching the benthos (Karlsson et al. 2009). Furthermore, Mývatn’s high benthic production sustains very large midge populations (peak larval densities exceeding $500,000 \text{ m}^{-2}$) that are themselves important drivers of benthic primary production (Herren et al. 2017; Phillips et al. 2019), as is the case for both midges and other benthic invertebrates in a variety of aquatic ecosystems (Largaespada et al. 2012; Hölker et al. 2015). However, water column phycocyanin concentrations were a strong predictor of the maximum potential GPP at high light, which suggests that pelagic production is greater than previously appreciated and may be a major contributor to temporal variation in overall GPP. While these data are suggestive of the relative contributions and variability of benthic and pelagic production, a formal partitioning of the two processes would require additional data (e.g., oxygen measurements at multiple depths) (Van de Bogert et al. 2007; Obrador et al. 2014). Partitioning of benthic and pelagic production has been attempted for some lakes (Vadeboncoeur et al. 2003; Van de Bogert et al. 2007; Obrador et al. 2014; Brothers et al. 2016) but is still quite limited, especially at temporal scales and resolutions necessary to understand how the relative contribution of these two processes changes through time.

This study illustrates the potential for temporal variation in P-I curves to vary through time and how modeling this variation can clarify the drivers of lake metabolism. Essential to this approach was high-resolution data spanning many years in conjunction with a new modeling approach that built on many recent advances in techniques for inferring lake metabolism from free-water DO measurements. Future work will benefit from continued growth in both areas, particularly from data that are both temporally and spatially extensive to help clarify the relative contribution of various physical and biological processes to lake metabolism.

References

- Ask, J., J. Karlsson, L. Persson, P. Ask, P. Byström, and M. Jansson. 2009. Terrestrial organic matter and light penetration: Effects on bacterial and primary production in lakes. *Limnol. Oceanogr.* **54**: 2034–2040. doi:10.4319/lo.2009.54.6.2034
- Attard, K. M., R. N. Glud, D. F. McGinnis, and S. Rysgaard. 2014. Seasonal rates of benthic primary production in a Greenland fjord measured by aquatic eddy correlation. *Limnol. Oceanogr.* **59**: 1555–1569. doi:10.4319/lo.2014.59.5.1555
- Batt, R. D., and S. R. Carpenter. 2012. Free-water lake metabolism: Addressing noisy time series with a Kalman filter:

- Kalman filter metabolism. *Limnol. Oceanogr. Methods* **10**: 20–30. doi:[10.4319/lom.2012.10.20](https://doi.org/10.4319/lom.2012.10.20)
- Behrenfeld, M. J., and P. G. Falkowski. 1997. A consumer's guide to phytoplankton primary productivity models. *Limnol. Oceanogr.* **42**: 1479–1491.
- Bergquist, A. M., and S. R. Carpenter. 1986. Limnetic herbivory: Effects on phytoplankton populations and primary production. *Ecology* **67**: 1351–1360. doi:[10.2307/1938691](https://doi.org/10.2307/1938691)
- Björnsson, H., and T. Jónsson. 2004. Climate and climatic variability at Lake Myvatn. *Aquat. Ecol.* **38**: 129–144. doi:[10.1023/B:AECO.0000032061.51508.e6](https://doi.org/10.1023/B:AECO.0000032061.51508.e6)
- Box, G. E., G. M. Jenkins, and G. C. Reinsel. 1994. Time series analysis: Forecasting and control, 3rd ed. Prentice Hall, Englewood Cliffs, New.
- Brothers, S., Y. Vadeboncoeur, and P. Sibley. 2016. Benthic algae compensate for phytoplankton losses in large aquatic ecosystems. *Glob. Chang. Biol.* **22**: 3865–3873. doi:[10.1111/gcb.13306](https://doi.org/10.1111/gcb.13306)
- Carpenter, B., A. Gelman, M. D. Hoffman, and others. 2017. Stan: A probabilistic programming language. *J. Stat. Softw.* **76**:1–32. doi:[10.18637/jss.v076.i01](https://doi.org/10.18637/jss.v076.i01)
- Carpenter, S. R., and J. F. Kitchell. 1984. Plankton community structure and limnetic primary production. *Am. Nat.* **124**: 159–172. doi:[10.1086/284261](https://doi.org/10.1086/284261)
- Carpenter, S. R., J. J. Cole, J. R. Hodgson, and others. 2001. Trophic cascades, nutrients, and lake productivity: Whole-lake experiments. *Ecol. Monogr.* **71**: 163–186. doi:[10.1890/0012-9615\(2001\)071\[0163:TCNALP\]2.0.CO;2](https://doi.org/10.1890/0012-9615(2001)071[0163:TCNALP]2.0.CO;2)
- Chapin, F. S., G. M. Woodwell, J. T. Randerson, and others. 2006. Reconciling carbon-cycle concepts, terminology, and methods. *Ecosystems* **9**: 1041–1050. doi:[10.1007/s10021-005-0105-7](https://doi.org/10.1007/s10021-005-0105-7)
- Clark, J. S. 2007. Models for ecological data: An introduction. Princeton Univ. Press.
- Cole, J. J., and N. F. Caraco. 1998. Atmospheric exchange of carbon dioxide in a low-wind oligotrophic lake measured by the addition of SF₆. *Limnol. Oceanogr.* **43**: 647–656. doi:[10.4319/lo.1998.43.4.0647](https://doi.org/10.4319/lo.1998.43.4.0647)
- Cole, J. J., S. R. Carpenter, M. L. Pace, M. C. V. de Bogert, J. L. Kitchell, and J. R. Hodgson. 2006. Differential support of lake food webs by three types of terrestrial organic carbon. *Ecol. Lett.* **9**: 558–568. doi:[10.1111/j.1461-0248.2006.00898.x](https://doi.org/10.1111/j.1461-0248.2006.00898.x)
- Cole, J. J., Y. T. Prairie, N. F. Caraco, and others. 2007. Plumbing the global carbon cycle: Integrating inland waters into the terrestrial carbon budget. *Ecosystems* **10**: 172–185. doi:[10.1007/s10021-006-9013-8](https://doi.org/10.1007/s10021-006-9013-8)
- Coloso, J. J., J. J. Cole, and M. L. Pace. 2011. Difficulty in discerning drivers of Lake ecosystem metabolism with high-frequency data. *Ecosystems* **14**: 935–948. doi:[10.1007/s10021-011-9455-5](https://doi.org/10.1007/s10021-011-9455-5)
- Crusius, J., and R. Wanninkhof. 2003. Gas transfer velocities measured at low wind speed over a lake. *Limnol. Oceanogr.* **48**: 1010–1017. doi:[10.4319/lo.2003.48.3.1010](https://doi.org/10.4319/lo.2003.48.3.1010)
- Davison, I. R. 1991. Environmental effects on algal photosynthesis: Temperature. *J. Phycol.* **27**: 2–8. doi:[10.1111/j.0022-3646.1991.00002.x](https://doi.org/10.1111/j.0022-3646.1991.00002.x)
- Del Giorgio, P. A., J. J. Cole, N. F. Caraco, and R. H. Peters. 1999. Linking planktonic biomass and metabolism to net gas fluxes in northern temperate lakes. *Ecology* **80**: 1422–1431. doi:[10.1890/0012-9658\(1999\)080\[1422:LPBAMT\]2.0.CO;2](https://doi.org/10.1890/0012-9658(1999)080[1422:LPBAMT]2.0.CO;2)
- Demars, B. O. L., G. M. Gíslason, J. S. Ólafsson, J. R. Manson, N. Friberg, J. M. Hood, J. J. D. Thompson, and T. E. Freitag. 2016. Impact of warming on CO₂ emissions from streams countered by aquatic photosynthesis. *Nat. Geosci.* **9**: 758–761. doi:[10.1038/ngeo2807](https://doi.org/10.1038/ngeo2807)
- Dubinsky, Z., and N. Stambler. 2009. Photoacclimation processes in phytoplankton: Mechanisms, consequences, and applications. *Aquat. Microb. Ecol.* **56**: 163–176. doi:[10.3354/ame01345](https://doi.org/10.3354/ame01345)
- Dugan, H. A., R. I. Woolway, A. B. Santoso, and others. 2016. Consequences of gas flux model choice on the interpretation of metabolic balance across 15 lakes. *Inland Waters* **6**: 581–592. doi:[10.1080/IW-6.4.836](https://doi.org/10.1080/IW-6.4.836)
- Edwards, K. F., C. A. Klausmeier, and E. Litchman. 2011. Evidence for a three-way trade-off between nitrogen and phosphorus competitive abilities and cell size in phytoplankton. *Ecology* **92**: 2085–2095.
- Edwards, K. F., M. K. Thomas, C. A. Klausmeier, and E. Litchman. 2015. Light and growth in marine phytoplankton: Allometric, taxonomic, and environmental variation: Light and growth in marine phytoplankton. *Limnol. Oceanogr.* **60**: 540–552. doi:[10.1002/lno.10033](https://doi.org/10.1002/lno.10033)
- Edwards, K. F., M. K. Thomas, C. A. Klausmeier, and E. Litchman. 2016. Phytoplankton growth and the interaction of light and temperature: A synthesis at the species and community level: Light-temperature interactions. *Limnol. Oceanogr.* **61**: 1232–1244. doi:[10.1002/lno.10282](https://doi.org/10.1002/lno.10282)
- Einarsson, Á., G. Stefánsdóttir, H. Jóhannesson, J. S. Ólafsson, G. M. Gíslason, I. Wakana, G. Gudbergsson, and A. Gardarsson. 2004. The ecology of Lake Myvatn and the river Laxá: Variation in space and time. *Aquatic Ecology* **38**: 317–348. doi:[10.1023/B:AECO.0000032090.72702.a9](https://doi.org/10.1023/B:AECO.0000032090.72702.a9)
- Falkowski, P. G. 1984. Physiological responses of phytoplankton to natural light regimes. *J. Plankton Res.* **6**: 295–307. doi:[10.1093/plankt/6.2.295](https://doi.org/10.1093/plankt/6.2.295)
- Fussmann, G. F. 2000. Crossing the Hopf bifurcation in a live predator-prey system. *Science* **290**: 1358–1360. doi:[10.1126/science.290.5495.1358](https://doi.org/10.1126/science.290.5495.1358)
- Gratton, C., J. Donaldson, and M. J. Vander Zanden. 2008. Ecosystem linkages between lakes and the surrounding terrestrial landscape in Northeast Iceland. *Ecosystems* **11**: 764–774. doi:[10.1007/s10021-008-9158-8](https://doi.org/10.1007/s10021-008-9158-8)
- Hanson, P. C., D. L. Bade, S. R. Carpenter, and T. K. Kratz. 2003. Lake metabolism: Relationships with dissolved organic carbon and phosphorus. *Limnol. Oceanogr.* **48**: 1112–1119. doi:[10.4319/lo.2003.48.3.1112](https://doi.org/10.4319/lo.2003.48.3.1112)
- Hanson, P. C., S. R. Carpenter, N. Kimura, C. Wu, S. P. Cornelius, and T. K. Kratz. 2008. Evaluation of metabolism

- models for free-water dissolved oxygen methods in lakes. *Limnol. Oceanogr. Methods* **6**: 454–465. doi:[10.4319/lom.2008.6.454](https://doi.org/10.4319/lom.2008.6.454)
- Hashioka, T., M. Vogt, Y. Yamanaka, and others. 2013. Phytoplankton competition during the spring bloom in four plankton functional type models. *Biogeosciences* **10**: 6833–6850. doi:<https://doi.org/10.5194/bg-10-6833-2013>
- Herrn, C. M., K. C. Webert, M. D. Drake, M. Jake Vander Zanden, Á. Einarsson, A. R. Ives, and C. Gratton. 2017. Positive feedback between chironomids and algae creates net mutualism between benthic primary consumers and producers. *Ecology* **98**: 447–455. doi:<https://doi.org/10.1002/ecy.1654>
- Hoellein, T. J., D. A. Bruesewitz, and D. C. Richardson. 2013. Revisiting Odum (1956): A synthesis of aquatic ecosystem metabolism. *Limnol. Oceanogr.* **58**: 2089–2100. doi:[10.4319/lo.2013.58.6.2089](https://doi.org/10.4319/lo.2013.58.6.2089)
- Holgerson, M. A., and P. A. Raymond. 2016. Large contribution to inland water CO₂ and CH₄ emissions from very small ponds. *Nat. Geosci.* **9**: 222–226. doi:[10.1038/ngeo2654](https://doi.org/10.1038/ngeo2654)
- Hölker, F., M. J. Vanni, J. J. Kuiper, and others. 2015. Tubedwelling invertebrates: Tiny ecosystem engineers have large effects in lake ecosystems. *Ecological Monographs* **85**: 333–351. doi:[10.1890/14-1160.1](https://doi.org/10.1890/14-1160.1)
- Holtgrieve, G. W., D. E. Schindler, T. A. Branch, and Z. T. A'mar. 2010. Simultaneous quantification of aquatic ecosystem metabolism and reaeration using a Bayesian statistical model of oxygen dynamics. *Limnol. Oceanogr.* **55**: 1047–1063. doi:[10.4319/lo.2010.55.3.1047](https://doi.org/10.4319/lo.2010.55.3.1047)
- Holtgrieve, G. W., and D. E. Schindler. 2011. Marine-derived nutrients, bioturbation, and ecosystem metabolism: Reconsidering the role of salmon in streams. *Ecology* **92**: 373–385. doi:[10.1890/09-1694.1](https://doi.org/10.1890/09-1694.1)
- Ives, A. R., Á. Einarsson, V. A. A. Jansen, and A. Gardarsson. 2008. High-amplitude fluctuations and alternative dynamical states of midges in Lake Myvatn. *Nature* **452**: 84–87. doi:[10.1038/nature06610](https://doi.org/10.1038/nature06610)
- Ive, A. R., and V. Dakos. 2012. Detecting dynamical changes in nonlinear time series using locally linear state-space models. *Ecosphere* **3**: art58. doi:[10.1890/ES11-00347.1](https://doi.org/10.1890/ES11-00347.1)
- Jassby, A. D., and T. Platt. 1976. Mathematical formulation of the relationship between photosynthesis and light for phytoplankton. *Limnol. Oceanogr.* **21**: 540–547. doi:[10.4319/lo.1976.21.4.0540](https://doi.org/10.4319/lo.1976.21.4.0540)
- Jónasson, P. M. 1979. The lake Mývatn ecosystem, Iceland. *Oikos* **32**: 289–305. doi:[10.2307/3544234](https://doi.org/10.2307/3544234)
- Karlsson, J., P. Byström, J. Ask, P. Ask, L. Persson, and M. Jansson. 2009. Light limitation of nutrient-poor lake ecosystems. *Nature* **460**: 506–509. doi:[10.1038/nature08179](https://doi.org/10.1038/nature08179)
- Klausmeier, C. A., and E. Litchman. 2001. Algal games: The vertical distribution of phytoplankton in poorly mixed water columns. *Limnol. Oceanogr.* **46**: 1998–2007. doi:[10.4319/lo.2001.46.8.1998](https://doi.org/10.4319/lo.2001.46.8.1998)
- Largaespada, C., F. Guichard, and P. Archambault. 2012. Metaecosystem engineering: Nutrient fluxes reveal intraspecific and interspecific feedbacks in fragmented mussel beds. *Ecology* **93**: 324–333. doi:[10.1890/10-2359.1](https://doi.org/10.1890/10-2359.1)
- Lindegaard, C., and P. M. Jónasson. 1979. Abundance, population dynamics and production of Zoobenthos in Lake Mývatn, Iceland. *Oikos* **32**: 202–227. doi:[10.2307/3544228](https://doi.org/10.2307/3544228)
- Long, M. H., J. E. Rheuban, P. Berg, and J. C. Zieman. 2012. A comparison and correction of light intensity loggers to photosynthetically active radiation sensors: Comparison of light loggers and PAR sensors. *Limnol. Oceanogr. Methods* **10**: 416–424. doi:[10.4319/lom.2012.10.416](https://doi.org/10.4319/lom.2012.10.416)
- Moore, C. M., D. J. Suggett, A. E. Hickman, Y.-N. Kim, J. F. Tweddle, J. Sharples, R. J. Geider, and P. M. Holligan. 2006. Phytoplankton photoacclimation and photoadaptation in response to environmental gradients in a shelf sea. *Limnol. Oceanogr.* **51**: 936–949. doi:[10.4319/lo.2006.51.2.0936](https://doi.org/10.4319/lo.2006.51.2.0936)
- Obrador, B., P. A. Staehr, and J. P. C. Christensen. 2014. Vertical patterns of metabolism in three contrasting stratified lakes. *Limnol. Oceanogr.* **59**: 1228–1240. doi:[10.4319/lo.2014.59.4.1228](https://doi.org/10.4319/lo.2014.59.4.1228)
- Odum, H. T. 1956. Primary production in flowing waters. *Limnol. Oceanogr.* **1**: 102–117. doi:[10.4319/lo.1956.1.2.0102](https://doi.org/10.4319/lo.1956.1.2.0102)
- Ólafsson, J. 1979. The chemistry of Lake Mývatn and river Laxá. *Oikos* **32**: 82–112. doi:[10.2307/3544222](https://doi.org/10.2307/3544222)
- Phillips, J. S., A. R. McCormick, Á. Einarsson, S. N. Grover, and A. R. Ives. 2019. Spatiotemporal variation in the sign and magnitude of ecosystem engineer effects on lake ecosystem production. *Ecosphere*. **10**:1–19. doi:[10.1002/ecs2.2760](https://doi.org/10.1002/ecs2.2760)
- Pinheiro, J., D. Bates, S. DebRoy, D. Sarkar, and R Core Team. 2018. nlme: Linear and nonlinear mixed effects models. R package version 3.1–137, URL: <https://CRAN.R-project.org/package=nlme>
- R Core Team. 2018. R: A language and environment for statistical computing. R Foundation for Statistical Computing.
- Randerson, J. T., F. S. Chapin, J. W. Harden, J. C. Neff, and M. E. Harmon. 2002. Net ecosystem production: A comprehensive measure of net carbon accumulation by ecosystems. *Ecol. Appl.* **12**: 937–947. doi:[10.2307/3061028](https://doi.org/10.2307/3061028)
- Raymond, P. A., J. Hartmann, R. Lauerwald, and others. 2013. Global carbon dioxide emissions from inland waters. *Nature* **503**: 355–359. doi:[10.1038/nature12760](https://doi.org/10.1038/nature12760)
- Richardson, D. C., C. C. Carey, D. A. Bruesewitz, and K. C. Weathers. 2017. Intra- and inter-annual variability in metabolism in an oligotrophic lake. *Aquat. Sci.* **79**: 319–333. doi:[10.1007/s00027-016-0499-7](https://doi.org/10.1007/s00027-016-0499-7)
- Sadro, S., C. E. Nelson, and J. M. Melack. 2011. Linking diel patterns in community respiration to bacterioplankton in an oligotrophic high-elevation lake. *Limnol. Oceanogr.* **56**: 540–550. doi:[10.4319/lo.2011.56.2.0540](https://doi.org/10.4319/lo.2011.56.2.0540)
- Schindler, D. E., K. Jankowski, Z. T. A'mar, and G. W. Holtgrieve. 2017. Two-stage metabolism inferred from diel

- oxygen dynamics in aquatic ecosystems. *Ecosphere* **8**:1–15. doi:10.1002/ecs2.1867
- Schwaderer, A. S., K. Yoshiyama, P. de Tezanos Pinto, N. G. Swenson, C. A. Klausmeier, and E. Litchman. 2011. Eco-evolutionary differences in light utilization traits and distributions of freshwater phytoplankton. *Limnol. Oceanogr.* **56**: 589–598. doi:10.4319/lo.2011.56.2.0589
- Solomon, C. T., D. A. Bruesewitz, D. C. Richardson, and others. 2013. Ecosystem respiration: Drivers of daily variability and background respiration in lakes around the globe. *Limnol. Oceanogr.* **58**: 849–866. doi:10.4319/lo.2013.58.3.0849
- Song, C., W. K. Dodds, J. Rüegg, and others. 2018. Continental-scale decrease in net primary productivity in streams due to climate warming. *Nat. Geosci.* **11**: 415. doi:10.1038/s41561-018-0125-5
- Staehr, P. A., D. Bade, M. C. Van de Bogert, G. R. Koch, C. Williamson, P. Hanson, J. J. Cole, and T. Kratz. 2010a. Lake metabolism and the diel oxygen technique: State of the science: Guideline for lake metabolism studies. *Limnol. Oceanogr. Methods* **8**: 628–644. doi:10.4319/lom.2010.8.0628
- Staehr, P. A., K. Sand-Jensen, A. L. Raun, B. Nilsson, and J. Kidmose. 2010b. Drivers of metabolism and net heterotrophy in contrasting lakes. *Limnol. Oceanogr.* **55**: 817–830. doi:10.4319/lo.2010.55.2.0817
- Staehr, P. A., L. S. Brighenti, M. Honti, J. Christensen, and K. C. Rose. 2016. Global patterns of light saturation and photoinhibition of lake primary production. *Inland Waters* **6**: 593–607. doi:10.1080/IW-6.4.888
- Stan Development Team. 2018. RStan: The R interface to Stan. R package version 2.18.2. <http://mc-stan.org/>
- Taranu, Z. E., I. Gregory-Eaves, P. R. Leavitt, and others. 2015. Acceleration of cyanobacterial dominance in north temperate-subarctic lakes during the Anthropocene. *Ecol. Lett.* **18**: 375–384. doi:10.1111/ele.12420
- Thimijan, R. W., and R. D. Heins. 1983. Photometric, radiometric, and quantum light units of measure a review of procedures for interconversion. *HortScience* **18**: 5.
- Thorp, J. H., and M. D. DeLong. 2002. Dominance of autochthonous autotrophic carbon in food webs of heterotrophic rivers. *Oikos* **96**: 543–550. doi:10.1034/j.1600-0706.2002.960315.x
- Vadeboncoeur, Y., M. J. Vander Zanden, and D. M. Lodge. 2002. Putting the lake back together: Reintegrating benthic pathways into Lake food web models lake ecologists tend to focus their research on pelagic energy pathways, but, from algae to fish, benthic organisms form an integral part of lake food webs. *Bioscience* **52**: 44–54. doi:10.1641/0006-3568(2002)052[0044:PTLBTR]2.0.CO;2
- Vadeboncoeur, Y., E. Jeppesen, M. J. Vander Zanden, H.-H. Schierup, K. Christoffersen, and D. M. Lodge. 2003. From Greenland to green lakes: Cultural eutrophication and the loss of benthic pathways in lakes. *Limnol. Oceanogr.* **48**: 1408–1418. doi:10.4319/lo.2003.48.4.1408
- Van de Bogert, M. C., S. R. Carpenter, J. J. Cole, and M. L. Pace. 2007. Assessing pelagic and benthic metabolism using free water measurements. *Limnol. Oceanogr. Methods* **5**: 145–155. doi:10.4319/lom.2007.5.145
- Vehtari, A., A. Gelman, and J. Gabry. 2017. Practical Bayesian model evaluation using leave-one-out cross-validation and WAIC. *Stat Comput* **27**: 1413–1432. doi:10.1007/s11222-016-9696-4
- Venkiteswaran, J. J., L. I. Wassenaar, and S. L. Schiff. 2007. Dynamics of dissolved oxygen isotopic ratios: A transient model to quantify primary production, community respiration, and air–water exchange in aquatic ecosystems. *Oecologia* **153**: 385–398. doi:10.1007/s00442-007-0744-9
- Vrede, T., A. Ballantyne, C. Mille-Lindblom, G. Algesten, C. Gudasz, S. Lindahl, and A. K. Brunberg. 2009. Effects of N : P loading ratios on phytoplankton community composition, primary production and N fixation in a eutrophic lake. *Freshwater Biol.* **54**: 331–344. doi:10.1111/j.1365-2427.2008.02118.x
- Yoshiyama, K., J. P. Mellard, E. Litchman, and C. A. Klausmeier. 2009. Phytoplankton competition for nutrients and light in a stratified water column. *Am. Nat.* **174**: 190–203. doi:10.1086/600113
- Zeng, Z., R. M. Nowierski, M. L. Taper, B. Dennis, and W. P. Kemp. 1998. Complex population dynamics in the real world: Modeling the influence of time-varying parameters and time lags. *Ecology* **79**: 2193–2209. doi:10.1890/0012-9658(1998)079[2193:CPDITR]2.0.CO;2

Acknowledgments

The data used in this manuscript were collected during routine sampling of Mývatn supported by National Science Foundation LTREB DEB-1556208 to Anthony R. Ives and the Mývatn Research Station directed by Árni Einarsson. This work was also funded by National Science Foundation Graduate Research Fellowship (DGE-1256259) supporting JSP. I would like to thank Jamie Botsch, Stephen Carpenter, Árni Einarsson, Anthony Ives, and Amanda McCormick for feedback on the analyses and manuscript.

Conflict of interest

The author has no conflicts of interest to declare.

Submitted 15 November 2018

Revised 29 May 2019

Accepted 15 August 2019

Associate editor: Paul Frost